Influence study of rail geometry and track properties on railway rolling noise

V. T. Andrés[a], J. Martínez-Casas[a,*], F. D. Denia[a], D. J. Thompson[b]

[a]*Instituto de Ingeniería Mecánica y Biomecánica, Universitat Politècnica de València, Camí de Vera, s/n 46022 Valencia, Spain*

[b]*Institute of Sound and Vibration Research, University of Southampton, Southampton SO17 1BJ, United Kingdom*

Abstract

Wheel/rail interaction generates an excitation due to the roughness present on the surface of both components that produces vibration and consequently rolling noise. In this work, the railway track properties that most influence rolling noise are identified and this influence is analysed to reduce noise emission. The acoustic calculation methodology consists of characterizing the wheel using finite element techniques and the track using periodic structure theory. The influence of the track properties on the sound radiation is analysed by means of statistical techniques applied to the acoustic power results of different track configurations. To achieve this, the rail cross-section geometry is parameterized and numerous simulations are carried out by modifying these geometric parameters and the viscoelastic properties of the track components. Considering the contribution of the wheel, rail and sleeper, the results obtained indicate that the total radiation can be reduced by up to 7.4 dB(A) through an optimal combination of the track design parameters, compared to the worst combination found. In particular, the rail pad stiffness is shown to be the most influential parameter in the sound radiation.

Keywords:
railway dynamics, track influence, rolling noise, wheel/rail interaction, sound radiation model, design of experiments, noise mitigation

1. Introduction

Railway transport is one of the most efficient, safe and environmentally friendly means of transport. However, it has been in the media focus in recent years due to the noise pollution generated. According to the World Health Organization, the noise pollution, in particular due to transport, is the second most damaging environmental factor for humans after air pollution [1]. Rolling noise is considered one of the main sources of railway sound radiation [2] and the most important in most situations [3]. This is produced as a consequence of the roughness of the wheel and rail surfaces which induces relative movement and thereby

*Corresponding author

Email addresses: vicanrui@upv.es (V. T. Andrés), jomarc12@mcm.upv.es (J. Martínez-Casas), fdenia@mcm.upv.es (F. D. Denia), djt@isvr.soton.ac.uk (D. J. Thompson)

generates dynamic contact forces. These excite the wheel and the track, causing a vibrational field that results in a radiated sound field. The frequency range of interest for rolling noise generation extends up to about 6 kHz [4]; above that frequency, the sound radiation falls abruptly due to the action of the contact filter [2, 5]. The main railway elements involved in rolling noise radiation are the sleepers, rails and wheels [6]. Furthermore, the frequency ranges of noise emission of each element exhibit some differences: the sleeper radiates at low and medium frequencies, the rail at medium and high frequencies and the wheel mainly at higher frequencies [6, 7].

Due to the great importance of railway noise pollution, especially in urban areas, different measures applied to the wheel and track have been proposed in the literature to mitigate rolling noise [8]. In regard to the wheel, Nielsen and Fredö [9] carried out a design of experiments with geometric parameters of the wheel and set up response surface models to find quieter designs; recently Garcia-Andrés *et al.* [10] proposed the use of optimization techniques on the wheel geometry with the same purpose; Jones and Thompson [11] studied the rolling noise generated by railway wheels with visco-elastic layers; Färm [12] tested the sound radiation for different circulation speeds when wheel dampers were included; Gramowski and Gerlach [13] presented a ready-to-market quiet wheelset design for freight traffic using vibration absorbers and Létourneaux et al. [14] proposed the use of wheel damping rings combined with rail dampers to attenuate both wheel and track noise components. In relation to the track, Thompson *et al.* [15] proposed the use of damping devices with viscoelastic materials and spring-mass type systems located both continuously and discretely along the circulation direction; Asmussen et al. [16] tested the reduction in the noise radiation of a track equipped with rail dampers for different circulation speeds and train types; Sun *et al.* [17] found large reductions in the radiation above 800 Hz by using this type of device and Gramowski and Suppin [18] assessed the impact of rail dampers on the long-term rail roughness development. The geometry of the rail cross-section has also been under consideration for the reduction of the radiated noise levels [19]. About the sleeper, Nielsen [7] concluded that the rail pad and ballast are the most important factors for the sleeper radiation, its geometry being of minor relevance. Regarding the rail pad, its design is an important task, since its properties have an opposite influence on the radiation of the rail and sleeper; Vincent *et al.* [20] carried out a parametric study of the influence of the rail pad stiffness and damping on sound radiation and showed that a stiff pad leads to reductions in rail noise and increases in sleeper noise. The optimal pad stiffness was shown to be at the high end of what is practical.

With the purpose of carrying out a detailed study of the influence of different parameters on rolling noise to mitigate sound radiation, a vibroacoustic model of the railway elements has been implemented and compared with the commercial package TWINS [21, 22]. A modal approach is considered for the wheel [23] and the track formulation is based on periodic structure theory [24]. Likewise, the rail cross-section geometry has been parametrized taking into account the European rails specified by the standard EN13674-1 [25] and, along with parameters describing the stiffness and damping of the rail pad and ballast, a design of experiments has been performed. A factorial design is proposed to analyse the influence and importance of these parameters in the sound radiation of the railway elements by means of ANOVA techniques [26] and using the methodology developed by Pratt [27].

The vibroacoustic model of the railway elements is presented in Section 2. Then, in Section 3, the design of experiments carried out and the analysis methodology to investigate

the influence of different parameters are described. Section 4 discusses the results and the main conclusions are summarized in Section 5.

2. Railway vibroacoustic model

2.1. Wheel model

A three-dimensional approach is adopted to model the dynamic behaviour of the wheel by the Finite Element Method (FEM), considering the wheel as a flexible solid with N degrees of freedom (dof's). Given the wheel geometry, three directions of motion are defined, namely: axial or out-of-plane, radial and circumferential. These three directions form the cylindrical coordinate system employed for the wheel.

A modal approach is adopted and the motion equation is formulated in the frequency domain. Wheel modeshapes can be characterized in accordance with the number of nodal lines (i.e. remaining at rest) in different directions [2]. On the one hand, nodal diameters are defined as stationary lines that traverse the wheel in radial direction through its centre; on the other hand, nodal circles are defined as nodal lines with tangential direction, forming a circle the centre of which coincides with the wheel axis. In [2] a relation between the number of nodal diameters n of a modeshape and its modal damping ratio ξ is proposed, so that vibration modes with $n = 0$ have $\xi = 10^{-3}$, modes with $n = 1$ have $\xi = 10^{-2}$ and modes with $n \geq 2$ have $\xi = 10^{-4}$.

The wheel vibrational field in the frequency domain is obtained by means of modal superposition, considering the contribution of each vibration mode to the response. Specifically, it is computed as the product of the interaction force and the frequency response function (FRF) of the wheel. This response can be formulated in terms of velocity (mobility), as follows:

$$Y_{jk}(\omega) = \mathrm{i}\omega \sum_{r=1}^{tr} \frac{\phi_{kr}\phi_{jr}}{\omega_r^2 - \omega^2 + 2\mathrm{i}\xi_r\omega_r\omega}, \tag{1}$$

$$v_j(\omega) = \sum_{i=1}^{nd} Y_{ji}(\omega)F_i(\omega), \tag{2}$$

where ω is the harmonic excitation frequency, $Y_{jk}(\omega)$ is the mobility measured in the jth dof when a unit force is applied in the kth dof, ω_r is the natural frequency of the rth vibration mode, ϕ_{kr} is the modal amplitude of the kth dof for the rth mode normalized to unit mass matrix and tr is the truncation or number of modes considered as basis for the wheel response $v_j(\omega)$, formulated in terms of velocity. The number of directions considered in the wheel/rail interaction problem is given by nd while $F_i(\omega)$ is the value of the contact force applied in the ith direction at the contact point, which is obtained as indicated in Section 2.3.

After solving the railway wheel dynamics, its acoustic radiation is computed by postprocessing the vibrational field on its surface. The radiation model employed in this work was developed by Thompson [28] and it establishes that wheel sound power is obtained as the sum of the power associated with each set of modes with the same number of nodal diameters n. This model is implemented in the commercial software TWINS and the details of the formulation can be found in [29]. The methodology consists of dividing the wheel surface

into a number of concentric annular surfaces delimited by two radii assuming that the radiation in axial direction is a consequence of the motion of those annular surfaces, considered of constant amplitude. Likewise, it is assumed that the radiation in radial direction is due to the wheel tyre motion, also considered of constant amplitude. The wheel acoustic power W^W, considering a finite number p of annular surfaces, is evaluated as follows:

$$W^W(\omega) = \rho c \sum_n \left(\sigma_{a,n}(\omega) \sum_{j=1}^{p} \left(S_{a,j} \overline{\widetilde{v^2}}_{a,j,n}(\omega) \right) + \sigma_{r,n}(\omega) S_r \overline{\widetilde{v^2}}_{r,n}(\omega) \right), \tag{3}$$

where ρ is the density of air, c is the speed of sound and the subscripts a and r make reference to the axial and radial contribution, respectively. Functions σ are the radiation ratios, that can be obtained numerically, and for which a number of fitting expressions can be found in reference [28]. The subscript j loops over the annular surfaces and $S_{a,j}$ and S_r are the projected axial and radial radiation surfaces, respectively. Finally, the projected squared velocities are averaged over time ($\widetilde{\ }$) and space ($\overline{\ }$) and they are defined for each annular surface in axial direction and for the tyre in radial direction.

2.2. Track model

The railway track considered in this work is formed by the rail, rail pad, sleeper and ballast. The rail is modelled as an infinite structure supported by the sleepers by means of the rail pads and ballast. The latter are modelled as viscoelastic material and the sleeper is considered a rigid solid. In this way, the rail is supported by a spring-mass-spring system so that the railway track is modelled as a continuous viscoelastic two-layer with uniform transverse section as shown in Fig. 1. The properties of the rail pad, sleeper and ballast are distributed per unit length; although this approach omits the effects associated with the pinned-pinned frequency, which are more significant for stiff rail pads, it is commonly used for noise predictions due to its simplicity [21]. In this model, no connection is considered between adjacent sleepers.

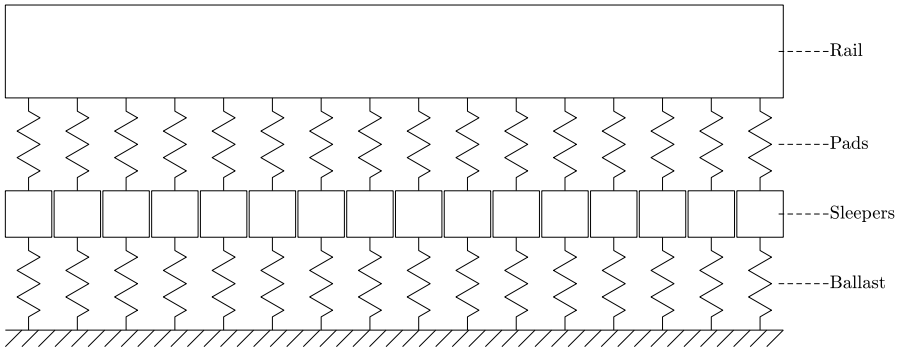

Fig. 1: Railway track model.

The track is modelled as an infinite structure through which, due to the wheel/rail interaction force, structural waves propagate in longitudinal direction (vehicle circulation direction); these waves form the basis for the track response. In order to obtain the variables that define these waves, the methodology proposed by Mead is employed [30]. This methodology

consists of analysing a track segment by means of finite element techniques; in this work a segment with a length of 10 mm is considered, as proposed by Thompson [24]. This segment along with its modelling is shown in Fig. 2. The rail section is discretized in a number of dof's, the sleeper section is modelled as a rigid solid and the rail pad and ballast as massless viscoelastic materials.

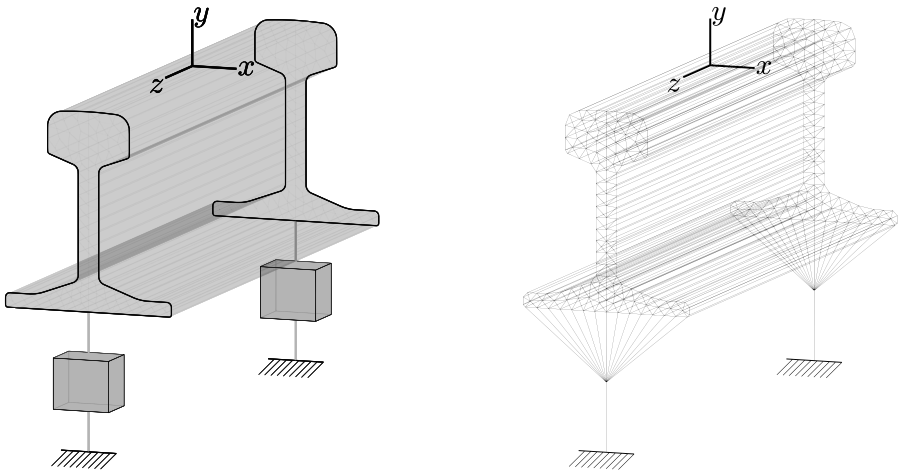

Fig. 2: Track segment (left) and its modelling (right). Figure out of scale in the longitudinal direction (z axis).

The treatment of the motion equation of the segment, in accordance with the methodology presented in [24, 30], allows the information to be known related to structural waves that propagate through the track; specifically, the waveshape ψ_r at any section point and the wavenumber k_r are known for the rth wave. By employing a cartesian reference system with origin in the contact point, where the x and y coordinates are contained in the track section and the z coordinate represents the longitudinal direction, then the displacement of any point on the track u is obtained as wave superposition:

$$u\left(x,y,z\right)=\sum_{r=1}^{m}A_r\psi_r\left(x,y\right)\mathrm{e}^{-\mathrm{i}k_r|z|}, \tag{4}$$

where m is the number of structural waves, which in the FE dynamic model is given by the number of dof's in the track section, and A_r is the generalized coordinate corresponding to the rth wave, that takes into account the contribution of this wave to the system response. By combining Eq. (4) and the motion equation of the segment, and considering continuity in displacements as well as balance of forces, the generalized coordinates are related to the input interaction force, as indicated in [24]. In Eq. (4) the frequency is implicit in the different functions defining the propagation. The FRF of the track is computed through Eq. (4) by applying a unit force and solving the generalized coordinates. After this, the Track Decay Rate (TDR) can be numerically evaluated similarly to the procedure described by the standard EN15461 [31]; the TDR characterizes the attenuation of the vibration on the track and, generally, has an inverse correlation with the track noise.

Regarding the track sound radiation, the contributions from both the rail and sleeper are considered. The acoustic model implemented for the rail is described in [29] and it is assumed a two-dimensional radiation of each rail cross-section, which is subsequently corrected to take into account the three-dimensional nature of the sound radiation. Bearing in mind that the rail acoustic power is proportional to the square velocity of its surface, then the power radiated by a differential of rail δz located at a distance z from the rail contact cross-section (the rail cross-section in which the wheel/rail contact occurs) due to the rth wave is

$$\delta W_r^R(z) = \widehat{W_r'^R}\ \mathrm{e}^{2\mathrm{Im}(k_r)|z|}\delta z, \tag{5}$$

where $\widehat{W_r'^R}$ is the power radiated by the rail contact cross-section per unit length ($\widehat{\ }$ indicates the contact cross-section and $'$ indicates per unit length). By integrating Eq. (5) over the rail (z coordinate from $-\infty$ to $+\infty$), the sound power associated with the rth wave is obtained. Finally, under the assumption that the different waves can be considered to radiate independently [29], the total rail power is the sum of each wave power, that is,

$$W^R = \sum_{r=1}^{m} \frac{\widehat{W_r'^R}}{-\mathrm{Im}(k_r)}. \tag{6}$$

In conclusion, since the response decay law of each wave is known, the rail radiation is obtained by computing the power of the cross-section and solving analytically the longitudinal direction. The sound radiation model of the rail contact cross-section $\widehat{W_r'^R}$ is based on Kirchhoff-Helmholtz integral equation [32], and detailed formulation can be found in appendix D of [29]. It is noted that this procedure consists of the two-dimensional estimation of the rail sound power and the analytical resolution of the longitudinal direction. This approach supposes a reasonable hypothesis for low decay rate waves; however, for high decay rate waves it is no longer valid. Accordingly, Thompson *et al.* [33] obtained numerically correction terms to consider the three-dimensional nature of the radiation of high decay rate waves, which are used here.

The same radiation model of the rail is employed for the sleeper, the other acoustically relevant element of the track. In this work, the sleeper is modelled as a rigid solid without considering the deformation of its section. Following the same procedure previously indicated for the rail and considering the sleeper motion in the cross-section in which the wheel/rail contact occurs, its sound power per unit length $\widehat{W_r'^S}$ is obtained and, applying Eq. (6), the sleeper acoustic power is calculated. Since the sleeper is in fact located discontinuously along the longitudinal direction, its radiation is adjusted by a factor b/d, where b is the width of the sleeper and d is the distance between sleepers.

2.3. Wheel/rail interaction

The wheel and rail surface roughness implies a source of excitation when the vehicle runs on the track due to the relative movement between both components. This excitation generates a vibrational field in the railway elements, producing rolling noise. Some typical roughness spectra are defined by the standard EN13979-1 [34]; particularly, in this work, the spectrum corresponding to wheels with cast iron brake blocks is considered. Also, the contact model proposed by Thompson is employed and details of the formulation can be found in

[2, 35]; from the roughness $\mathbf{r}$, which is assumed to have content only in vertical direction, the rail/wheel interaction force $\mathbf{F}$ is obtained solving the system

$$\left(\mathbf{H}^W + \mathbf{H}^C + \mathbf{H}^R\right)\mathbf{F} = \mathbf{r}, \tag{7}$$

where $\mathbf{H}^W$, $\mathbf{H}^C$ and $\mathbf{H}^R$ are the receptances in matrix form defined in the contact point for the wheel, contact and rail, respectively. For the wheel and rail receptance, calculation details have been presented in Section 2.1 and Section 2.2, respectively; contact receptance model is detailed in [2]. In this work, the interaction problem considers vertical and lateral directions and it is assumed that there is no steady state creepage superimposed on the dynamic motion. Likewise, the contact filter model developed by Remington [5] is included using the simplified form presented by Thompson [2]. The implementation of the model described in this Section has been verified by extensive comparisons with TWINS [21, 22].

3. Design of experiments

3.1. Design set up

The formulation presented in Section 2 has been implemented in order to analyse the influence of the properties of the railway components on their sound radiation. Regarding the wheel, Nielsen and Fredö [9] parametrized its geometry and they carried out a study of the influence of the geometric parameters on the acoustic radiation. In a recent work, Garcia-Andrés *et al.* [10] performed a geometric optimization of the wheel by using genetic algorithms to reduce rolling noise.

This work focuses on the influence of track properties on rolling noise. Specifically, the influence of the rail geometry and viscoelastic properties of the rail pad and ballast on the rail, sleeper and wheel sound radiation is studied. To this end, firstly, the rail cross-section is parameterized taking into account six main variables and bounds of each one are established; similarly, the viscoelastic properties of the pad and ballast are considered through four variables with their corresponding bounds. These ten design variables are shown in Fig. 3. Subsequently, a design of experiments and an ANOVA [26] on the results are performed, looking for a regression model that fits the calculated acoustic power. If the regression model is good enough, the analysis of the regression coefficents makes it possible to know the influence of the different contributing variables on the response variable, that is, on the railway sound radiation.

Regarding the pad and ballast stiffness, for simplicity the ratio between the lateral and vertical components is fixed: 1/13 for pad and 1/2 for ballast [4, 20]. Thus, variables k_{Pad} and $k_{Ballast}$ refer hereinafter to the vertical component of the pad and ballast stiffness, respectively. Likewise, structural damping of pad and ballast is considered through damping loss factors η_{Pad} and $\eta_{Ballast}$, respectively. The ranges of application of each design variable are shown in Table 1. The geometric parameter bounds are established based on the minimum and maximum dimensions that appear on the European rails specified by the standard EN13674-1 [25]. The viscoelastic parameter bounds are set according to the literature: values of k_{Pad} used in the European railway networks are specified in [20], limits of $k_{Ballast}$ are established to determine its influence on the vehicle/track interaction in [36] and the track dynamic behaviour at high frequencies is analysed for, among other parameters, different values of η_{Pad} and $\eta_{Ballast}$ in [37].

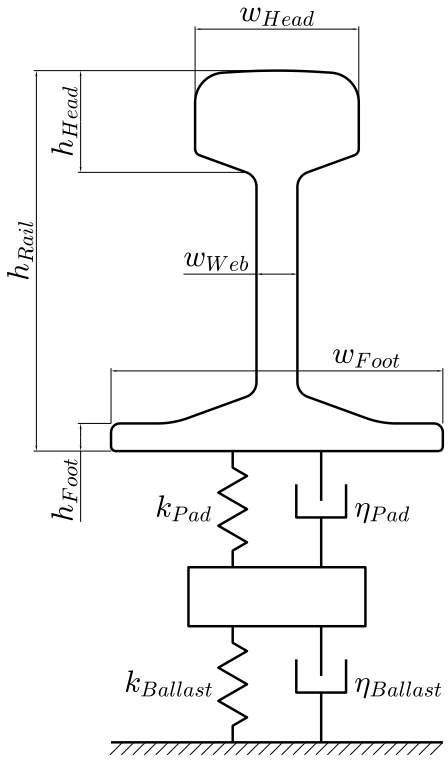

Fig. 3: Design variables of rail cross-section geometry and track properties.

3.2. Influence analysis methodology

In order to analyse the influence of the aforementioned ten parameters on the sound radiation of the rail, sleeper and wheel, a factorial design M^{10} without repetitions is proposed, M being the number of levels or values that each variable takes, covering all combinations of those levels in the parameters. An ANOVA is performed on the results of the simulations, modifying the effects to be considered to ensure their statistical significance on the sound power $SWL_{\sum}$, quantified by adding the energy contained in the frequency spectrum and it is expressed in decibels, that is,

$$SWL_{\sum} = 10 \log_{10} \left(\sum_{i=1}^{n_{bands}} 10^{\frac{SWL_i}{10}} \right), \tag{8}$$

where subscript i loops into the frequency one-third octave bands in which radiation is studied, n_{bands} is the number of one-third octave bands and SWL_i is the sound power level of the ith one-third octave band, obtained according to the procedure described by the standard EN13979-1 [34], which includes the effect of the contact filter and the A-weighting filter to consider the human ear perception [38].

This work not only seeks to determine the influence of each parameter on the response variable, but also to define its importance. For this purpose, the technique developed by Pratt [27], widely described by Thomas *et al.* [39, 40], is applied. The methodology allows the importance to be determined of each contributing variable from the set of samples obtained

Table 1: Design variables bounds.

Design variable	Lower bound	Upper bound
h_{Foot} [mm]	8	15
h_{Head} [mm]	39	49
h_{Rail} [mm]	142	172
w_{Foot} [mm]	120	150
w_{Head} [mm]	62	75
w_{Web} [mm]	14	20
k_{Pad} [MN/m]	130	1300
η_{Pad} [-]	0.25	0.5
$k_{Ballast}$ [MN/m]	40	100
$\eta_{Ballast}$ [-]	1	2

from the calculation of the factorial design. For these samples, a polynomial regression for the sound power of each railway element is performed where the response variable contains the radiation from each combination in the design of experiments after a standarization of the vector to null mean and unit norm, such that

$$\widehat{\mathbf{y}} = \sum_j \beta_j \mathbf{x}_j, \tag{9}$$

where $\widehat{\mathbf{y}}$ contains the response variable adjusted by least squares for each sample, $\mathbf{x}_j$ contains the standarized jth effect for each sample and β_j is the standarized regression coefficient for the jth effect. An effect might be a simple parameter, the interaction between parameters or the exponent of a parameter. In Eq. (9), orthogonal components of $\beta_j \mathbf{x}_j$ to $\widehat{\mathbf{y}}$ sum to zero and their projections onto $\widehat{\mathbf{y}}$ sum to precisely $\|\widehat{\mathbf{y}}\|$, $\|\ \|$ being the Euclidean norm. Therefore, these projections represent the importance of each effect on the response variable. The projection of the jth effect onto the adjusted response variable $\mathbf{P}_{\widehat{\mathbf{y}}}(\beta_j \mathbf{x}_j)$ is calculated as

$$\mathbf{P}_{\widehat{\mathbf{y}}}(\beta_j \mathbf{x}_j) = \frac{\widehat{\mathbf{y}} \cdot \beta_j \mathbf{x}_j}{\|\widehat{\mathbf{y}}\|} \frac{\widehat{\mathbf{y}}}{\|\widehat{\mathbf{y}}\|}. \tag{10}$$

Pratt [27] defined the relative importance of the jth effect as the ratio between the length of this projection and the length of $\widehat{\mathbf{y}}$. Thus, the summation of the relative importances defined by Pratt is unity. In this work, the importance of an effect is redefined as the proportion of variance in the response variable that it explains; in this context, the variance explained by the regression considering all the effects is the coefficient of determination R^2 of the regression model. The importance of an effect d_j is

$$d_j = \widehat{\mathbf{y}} \cdot \beta_j \mathbf{x}_j, \tag{11}$$

so that

$$\sum_j d_j = R^2. \tag{12}$$

4. Results

In this section, the influence of the track on sound radiation is analysed. Initially, a 3^{10} factorial design is proposed, considering three levels of each parameter corresponding to the minimum, medium and maximum values of its range (see Table 1). For each combination, by means of the implemented tool, the vibroacoustic problem is solved; to do this, the rail cross-section geometry is created, the dynamic wheel and track FE models are generated, the interaction between the two is resolved and the sound radiation of each railway element is calculated. An ANOVA with the significant effects is performed on the results and the Pratt methodology, described in Section 3.2, is applied to determine the variance explanation of each effect. By using this technique, the design variables influencing the sound power of each railway element are established. For each element, in order to have a greater spectrum of the noise range with respect to the variation of the most important parameters, this analysis procedure is repeated performing another factorial design with more levels of the contributing variables.

The results are expressed as the sound power due to one wheel and the associated track vibration. The following calculation parameters are considered fixed:

- A wheel with a straight web and a diameter of 900 mm, as well as a mass of 330 kg and a S1002 profile.
- A damping loss factor of 0.02 for the rail.
- A distance between sleepers of 0.6 m and a half sleeper with dimensions of 0.84 m in length (x direction), 0.22 m in height (y direction) and 0.25 m in bottom and top width (z direction), and with a mass of 122 kg.
- A vehicle speed of 80 km/h, a vertical static load of 50 kN per wheel and a roughness spectrum defined by the standard EN13979-1 corresponding to a wheel with cast iron brake blocks.

4.1. Influence on rail radiation

From the initial study, applying the Pratt methodology, the proportion of variance in rail radiation explained by each effect is determined, as well as the cumulative proportion. The variance explained by the more relevant effects is shown in Fig. 4 (colour black); the importance of the remaining effects is summed and represented as 'Rest'. In the context of the current investigation, the most important variables are identified as: w_{Foot}, k_{Pad} and η_{Pad}. Therefore, the sound power variation due to the other variables is considered negligible. In comparison to the three aforementioned variables, rail cross-section geometry barely affects

track dynamics in the frequency range of rail radiation (from 500 Hz to 2 kHz), so that the geometric parameters are not important design variables except w_{Foot}; the rail foot width is important since it alters the radiation ratio of the rail [2] and also its surface area has high velocities of vibration at higher frequencies. In this frequency range, the track behaviour is governed by the rail pad, so its stiffness and damping are important parameters in the rail radiation. Regarding the ballast, it is a component that influences the track dynamics below the frequency range in which the rail radiation is important. With these relevant design variables, a design of experiment is carried out considering eight levels of each one, that is, a design with 8^3 combinations. Again, the proportion of variance explained by each effect in the polynomial regression model is determined, which is shown in Fig. 4 (colour blue) along with the cumulative proportion. The regression model has $R^2 = 99.9$ % and the most important parameter is again the rail pad stiffness, which explains 93.7 % of the variance in the rail sound power.

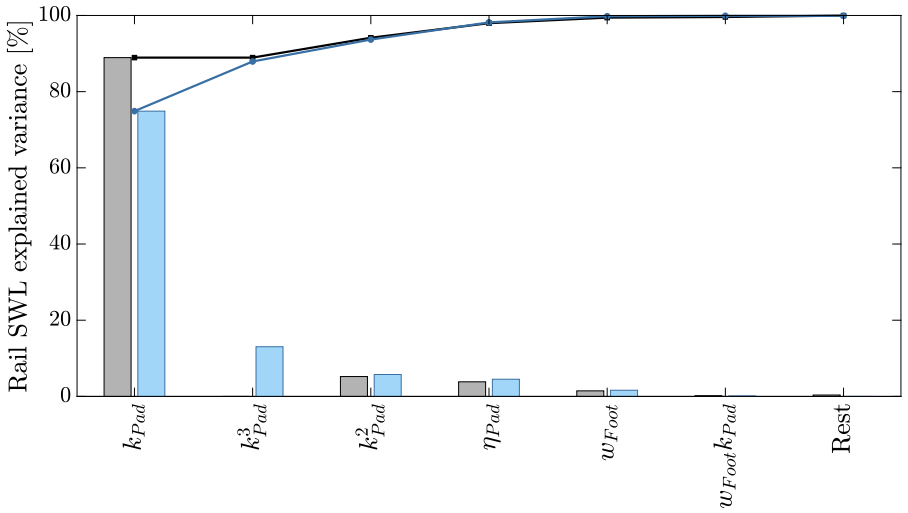

Fig. 4: Effect importance (bar) and cummulative value (line) on rail radiation: initial study (black) and refined study (blue).

The polynomial regression model is as follows:

$$SWL_{\sum,Rail} = a_0 + a_1 k_{Pad} + a_2 k_{Pad}^2 + a_3 k_{Pad}^3 + a_4 \eta_{Pad} + a_5 w_{Foot} + a_6 w_{Foot} k_{Pad}, \tag{13}$$

the coefficients of which are given in Table 2. In Fig. 5 a comparison between the rail sound power calculated with the implemented vibroacoustic tool and the prediction with the regression model is shown. The good approximation provided by the model makes it possible to analyse the coefficients of the regression and establish trends of the contributing variables on the rail sound radiation. It should be noted that the sound radiation calculation of the 8^3 design of experiments takes approximately 20 hours (140 seconds per combination) while the time associated with the prediction from Eq. (13) is negligible; the numerical simulations are carried out in a PC running with an ®Intel i7-9700 processor with 64 GB RAM.

The rail pad stiffness has a non-linear influence on the rail radiation. Although quadratic and cubic terms involving this parameter appear in the polynomial regression, this fact does

Table 2: Coefficients* of rail sound power regression model presented in Eq. (13).

a_0	a_1	a_2	a_3	a_4	a_5	a_6
99.5	$-2.3 \cdot 10^{-2}$	$2 \cdot 10^{-5}$	$-5.7 \cdot 10^{-9}$	-10.7	$8 \cdot 10^{-2}$	$-3.7 \cdot 10^{-5}$

*Stiffness in MN/m, geometric parameters in mm and sound power in dB(A) re 1 pW.

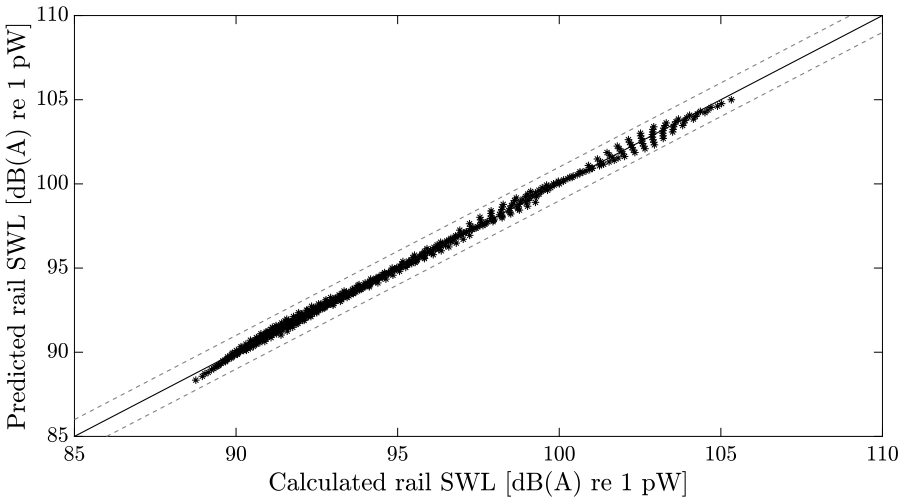

Fig. 5: Predicted vs calculated rail SWL. ——: reference line; - - -: 1 dB(A) deviation; ∗: each track design.

not affect the importance of the other effects due to the independence obtained through the design of experiments. Thus, the rail pad stiffness is the most important parameter; as it increases, the vibrational field of the rail extends over a shorter length and, consequently, its radiation is reduced. The same happens when increasing the pad damping loss factor, although its range of realistic values is smaller. Also, reducing the rail foot width results in lower sound emission as it reduces the radiation ratio and the radiation area which, as mentioned above, is where the higher velocities of vibration appear. The interaction effect $w_{Foot}k_{Pad}$ represents the loss of importance of the rail foot width as the rail pad stiffness is increased due to the lower noise levels radiated; this phenomenon can be appreciated by modifying the regression model and introducing the influence of k_{Pad} implicitly:

$$SWL_{\sum,Rail} = b_0(k_{Pad}) + b_1(k_{Pad})w_{Foot} + b_2\eta_{Pad}, \tag{14}$$

where the influence of w_{Foot} is defined by means of the coefficient b_1, dependence of which on k_{Pad} is shown in Fig. 6. This coefficient is always positive, that is, reducing the rail foot width leads to lower rail radiation; however, its influence is reduced as the pad stiffness is increased. Note that a narrower rail foot would imply a greater pressure level on the rail pad and, given the non-linear nature of this material, its stiffness would increase [41]. This phenomenon would have, on the interaction effect $w_{Foot}k_{Pad}$, an influence of opposite sign to that previously attributed, so that it would increase the value of the coefficient a_6 in Eq. (13) and Table 2. Consequently, this would yield an increase of the slope in Fig. 6. However,

this effect has not been considered in the present study.

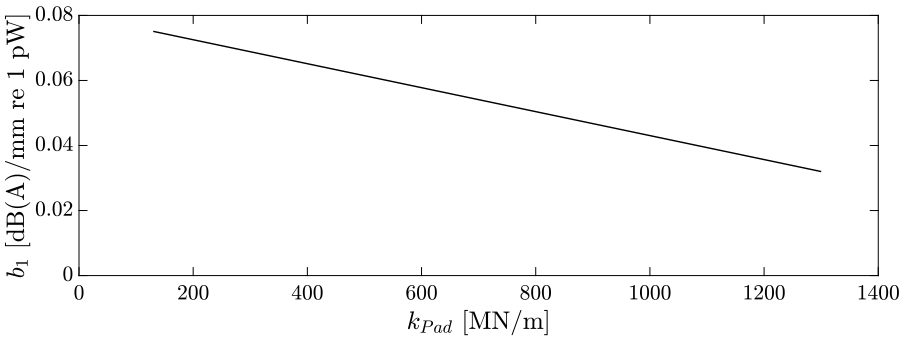

Fig. 6: Coefficient b_1 value from Eq. (14) as a function of k_{Pad}.

Finally, the great variability in the rail sound power results should be noted, with a difference between the best and the worst combination of 16.6 dB(A). The optimal solution according to the regression model corresponds to the maximum value of k_{Pad}, 1300 MN/m in vertical direction and 100 MN/m in lateral direction, the maximum value of η_{Pad}, 0.5, and the minimum value of w_{Foot}, 120 mm, which implies a rail sound power of 88.8 dB(A).

4.2. Influence on sleeper radiation

The same procedure is carried out with the sleeper sound radiation being the response variable. Firstly, the importance of each effect from the initial study is determined, which is shown in Fig. 7 (colour black); the more relevant parameters are determined: k_{Pad}, η_{Pad}, $k_{Ballast}$ and $\eta_{Ballast}$. In the frequency range in which the sleeper radiation is important (below 750 Hz), track dynamics and particularly sleeper dynamics are governed by the rail pad and ballast, whereas the rail cross-section geometry has a negligible influence. Considering these four contributing variables, a design of experiments with 5^4 combinations is proposed. Again, the Pratt methodology is applied on the simulation results, determining the importance of each significant effect, which is shown in Fig. 7 (colour blue). In this case, the regression model has $R^2 = 99.3$ %, k_{Pad} being the most important design variable again. The regression is given as

$$\begin{aligned} SWL_{\sum,Sleeper} =& a_0 + a_1 k_{Pad} + a_2 k_{Pad}^2 + a_3 k_{Pad}^3 + a_4 \eta_{Ballast} + a_5 k_{Ballast} + a_6 \eta_{Pad} + \\ &+ a_7 k_{Pad} k_{Ballast} + a_8 k_{Pad} \eta_{Ballast} + a_9 k_{Pad} \eta_{Pad}, \end{aligned} \tag{15}$$

and the values of the corresponding coefficients are provided in Table 3. From the 5^4 design of experiments, the calculated sleeper sound power and its prediction by Eq. (15) are compared in Fig. 8.

Unlike the rail radiation, the higher the pad stiffness is, the more sound the sleeper radiates since the rail vibration is transmitted to a greater extent to the sleeper. On the contrary, the higher the ballast stiffness, the less the sleeper vibrates and, consequently, the less the sleeper radiates. Regarding the damping loss factors of pad and ballast, increasing them leads to a reduction in the sleeper sound power. Note that the rail pad stiffness not only

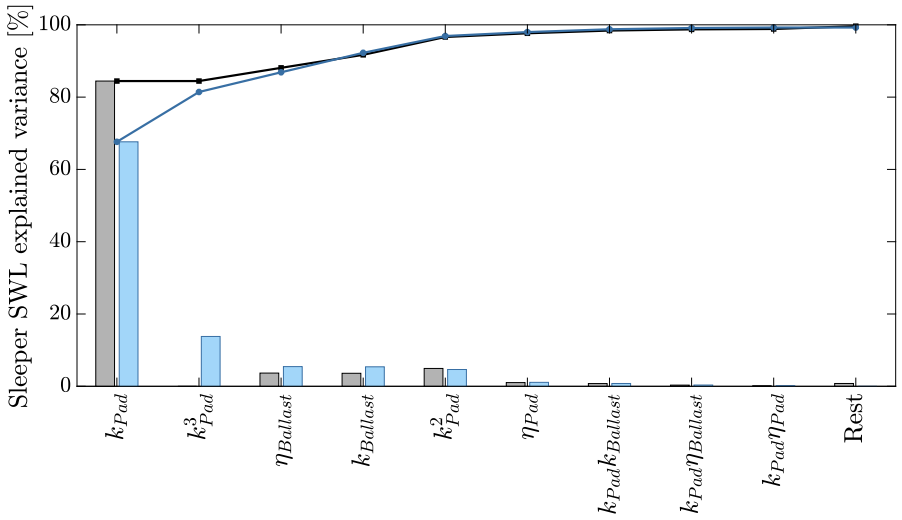

Fig. 7: Effect importance (bar) and cummulative value (line) on sleeper radiation: initial study (black) and refined study (blue).

Table 3: Coefficients* of sleeper sound power regression model presented in Eq. (15).

a_0	a_1	a_2	a_3	a_4
92.8	$1.8 \cdot 10^{-2}$	$-1.1 \cdot 10^{-5}$	$3.3 \cdot 10^{-9}$	-0.99

a_5	a_6	a_7	a_8	a_9
$-1 \cdot 10^{-2}$	-5	$-2.7 \cdot 10^{-5}$	$-1.1 \cdot 10^{-3}$	$2.6 \cdot 10^{-3}$

*Stiffness in MN/m and sound power in dB(A) re 1 pW.

dominates the sleeper radiation, but also takes part in the influence of the other parameters through the interaction effects. In order to analyse this dependence, a polynomial fit is proposed in which the simple effect of k_{Pad} disappears, including it in the coefficients:

$$SWL_{\sum,Sleeper} = b_0(k_{Pad}) + b_1(k_{Pad})k_{Ballast} + b_2(k_{Pad})\eta_{Ballast} + b_3(k_{Pad})\eta_{Pad}. \quad (16)$$

Fig. 9 shows the dependence of the coefficients in Eq. (16) with the rail pad stiffness. All of them are negative for any value of k_{Pad}, so that, independently of it, increasing the ballast stiffness or the damping loss factors leads to a reduction in the sleeper sound radiation. However, a higher value of k_{Pad} increases the influence of $k_{Ballast}$ and $\eta_{Ballast}$ and reduces the influence of η_{Pad}; this phenomenon represents the loss of influence of the rail pad as its stiffness increases above that of the ballast.

On balance, the sleeper radiation shows a variation between the best and the worst combination of 11 dB(A). The optimal case corresponds to the minimum value of k_{Pad}, 130 MN/m in vertical direction and 10 MN/m in lateral direction, the maximum value of $k_{Ballast}$,

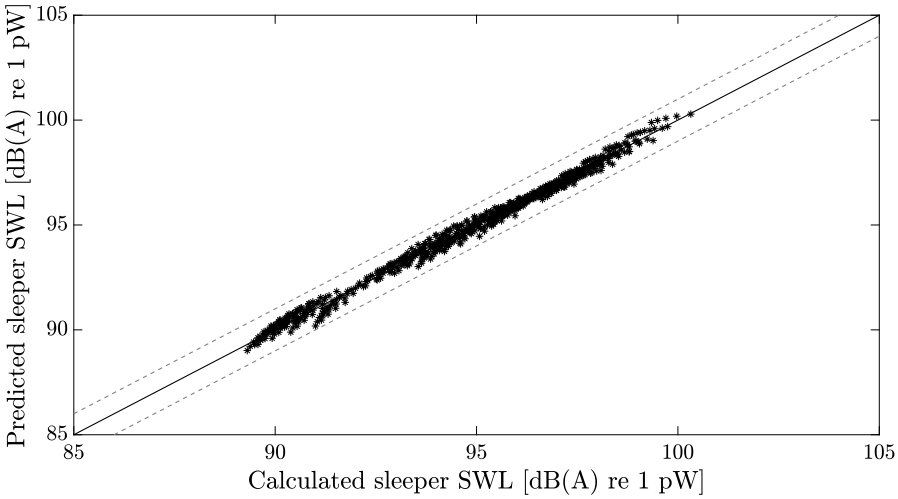

Fig. 8: Predicted vs calculated sleeper SWL. ——: reference line; - - -: 1 dB(A) deviation; ∗: each track design.

100 MN/m in vertical direction and 50 MN/m in lateral direction, the maximum value of $\eta_{Ballast}$, 2, and the maximum value of η_{Pad}, 0.5, with a sleeper sound power of 89.3 dB(A).

4.3. Influence on wheel radiation

Since the wheel properties are fixed in this work, its vibration depends exclusively on the contact forces, which have an inverse dependence on the combined receptance of the system at the contact point, the sum of the rail, wheel and contact receptances, as indicated in Eq. (7). Thus, the track parameters that influence the wheel radiation are those which give a notable modification of the rail contact point receptances in the frequency range in which the wheel radiation is important (> 1.5 kHz). The railway wheel, being a finite structure, has a high number of natural frequencies and vibration modes (i.e. resonances) in that frequency range. Changes in the contact force influence the wheel vibration to a lesser or greater extent depending on the distribution of these resonances. For this reason, the influence of the track parameters on the wheel radiation might depend on the studied wheel. This section looks for trends applicable to any railway wheel, indicating which results are sensitive to the properties of the wheel.

The important parameters identified that influence the wheel radiation are the rail pad stiffness and all the rail cross-section geometric factors. Changes in the rail pad stiffness might modify the rail contact point receptances up to 3 kHz, whereas the pad damping loss factor, ballast stiffness and ballast damping loss factor do not influence significatively the rail receptances above 1.5 kHz. Therefore, these three parameters (η_{Pad}, $k_{Ballast}$ and $\eta_{Ballast}$) have a negligible effect on the wheel sound power. Although the wheel radiation generally occurs at frequencies above 1.5 kHz, these variables might influence the sound radiation of highly flexible railway wheels with acoustically predominant vibration modes in the low and medium frequency range. However, the trend to optimize the railway wheel in terms of noise is to stiffen it, increasing its natural frequencies and shifting the radiation to high frequencies [10].

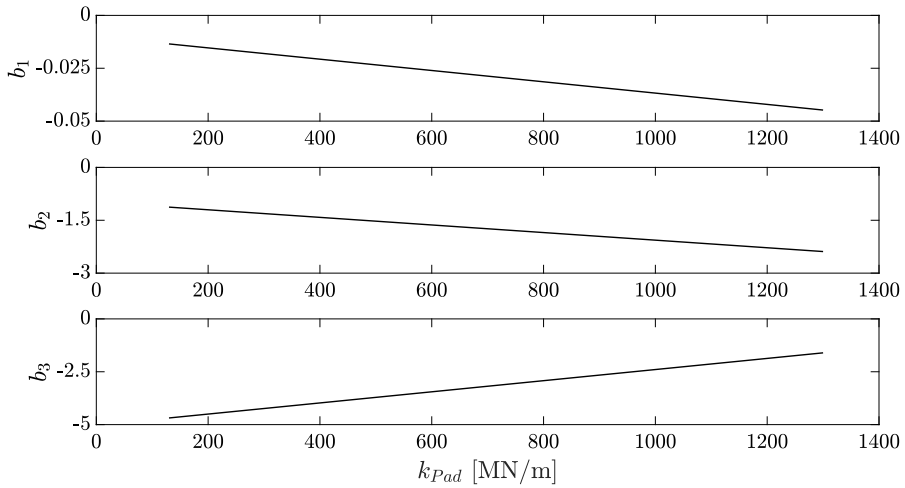

Fig. 9: Coefficient values from Eq. (16) as a function of k_{Pad}. b_1 has units of dB(A)/(MN/m) and b_2 and b_3 of dB(A).

In contrast to what it might appear, an increase in the rail pad stiffness reduces the wheel radiation. By stiffening the pad while keeping the mass of the track constant, its associated resonance frequency is increased and, as a result, the contact force magnitude decreases in the frequency range in which the wheel radiation is important. Regarding the rail geometric parameters, their influence might depend on the railway wheel considered. Generally, if the rail cross-section dimensions are reduced this will give a lower section stiffness and consequently lead to an increase in the magnitude of the rail contact point receptances. This reduces the contact force magnitude and wheel sound power.

In any case, since wheel properties are not modified, less variance is found in its sound radiation compared to the rail and sleeper. Specifically, the difference between the best and the worst combination is 3.3 dB(A), in contrast to 16.6 dB(A) for the rail and 11 dB(A) for the sleeper. The optimal combination for the wheel radiation is obtained generally with the maximum value of k_{Pad} and the minimum values of the rail geometric parameters. For the studied wheel, this combination implies a wheel sound power of 94.3 dB(A).

4.4. Influence on total radiation

From the initial design of experiments for the total sound radiation, the proportion of variance explained by each significant effect is determined, which is shown in Fig. 10 (colour black); in the context of the current investigation, the total sound radiation is influenced by the following design variables: w_{Foot}, k_{Pad}, η_{Pad}, $k_{Ballast}$ and $\eta_{Ballast}$. The rail pad properties influence the noise of all components, therefore being important in the total radiation. The ballast properties, which play an important role in the sleeper radiation, also appear as contributing variables. The rail foot width affects the radiation of the rail and, the rail power being the one that presents the highest variability, it is an important parameter in the total noise. Lastly, the remaining geometric parameters only influence the wheel radiation, variability of which, much less than that of the rail and sleeper, is mainly explained by the rail pad stiffness; therefore, they do not appear as important contributing variables in the total radiation.

With these five important parameters, a design of experiments with 5^5 combinations is carried out. The importance of the design variables in terms of explaining variability is determined and shown in Fig. 10 (colour blue). The regression model is given by

$$\begin{aligned} SWL_{\sum,Total} =& a_0 + a_1 k_{Pad} + a_2 k_{Pad}^2 + a_3 k_{Pad}^3 + a_4 \eta_{Pad} + a_5 w_{Foot} + a_6 k_{Ballast} + \\ &+ a_7 \eta_{Ballast} + a_8 w_{Foot} k_{Pad} + a_9 k_{Pad} k_{Ballast} + a_{10} k_{Pad} \eta_{Pad} + \\ &+ a_{11} k_{Pad} \eta_{Ballast}, \end{aligned} \tag{17}$$

and the values of the corresponding coefficients are provided in Table 4; it has $R^2 = 99.4$ %. The prediction carried out with this model is compared with the calculated results in Fig. 11. Given the good approximation provided by the regression model, the analysis of its coefficients allows the influence of the design variables on the total noise to be determined.

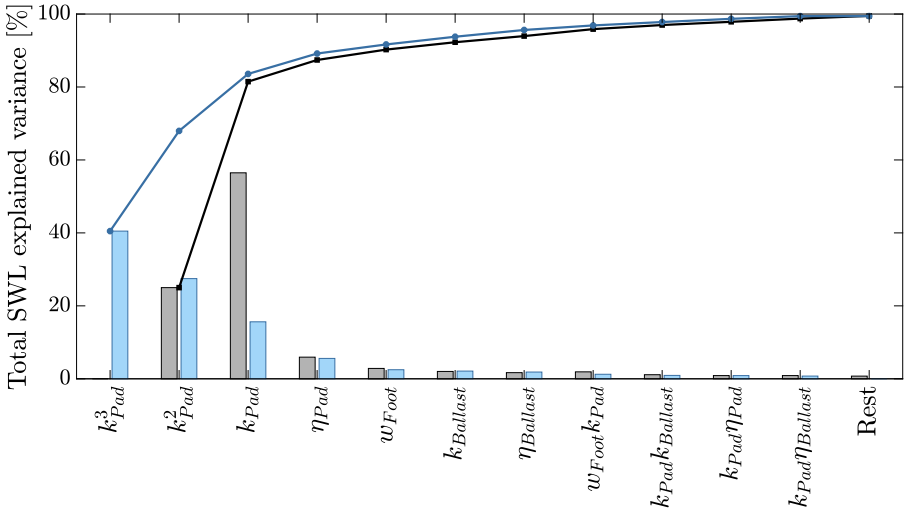

Fig. 10: Effect importance (bar) and cummulative value (line) on total radiation: initial study (black) and refined study (blue).

Table 4: Coefficients* of total sound power regression model presented in Eq. (17).

a_0	a_1	a_2	a_3	a_4	a_5
101.2	$-1.4 \cdot 10^{-2}$	$2.2 \cdot 10^{-5}$	$-7.2 \cdot 10^{-9}$	-7.6	$5.6 \cdot 10^{-2}$

a_6	a_7	a_8	a_9	a_{10}	a_{11}
$1.7 \cdot 10^{-3}$	$6.3 \cdot 10^{-2}$	$-4.3 \cdot 10^{-5}$	$-1.9 \cdot 10^{-5}$	$4.3 \cdot 10^{-3}$	$-1 \cdot 10^{-3}$

*Stiffness in MN/m, geometric parameters in mm and sound power in dB(A) re 1 pW.

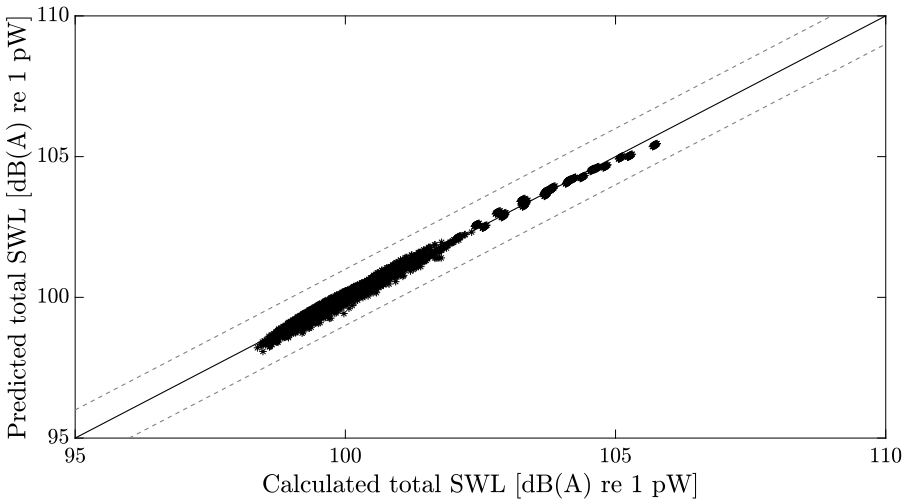

Fig. 11: Predicted vs calculated total SWL. ——: reference line; - - -: 1 dB(A) deviation; $*$: each track design.

The rail pad stiffness is shown to be the most important parameter, explaining 83.6 % of the noise variance (without considering the interaction effects). Increasing it leads to a reduction in the rail and wheel noise and an increase in the sleeper noise; for the total noise, at low rail pad stiffnesses the reduction in the rail by increasing it predominates over the increase in the sleeper noise, but at high stiffnesses there is a balance between the three components. This phenomenon is shown in Fig. 12, where it is observed that the highest sound mitigation occurs for intermediate/high values of the rail pad stiffness. Increasing the rail pad damping loss factor leads to a reduction of the rail and sleeper sound radiation and thus of the total acoustic power. Regarding the ballast, increasing its stiffness and damping reduces the sleeper radiation as seen previously and, although coefficients a_6 and a_7 in Eq. (17) are positive, it also reduces the total radiation due to the contribution of the interaction effects $k_{Pad}k_{Ballast}$ and $k_{Pad}\eta_{Ballast}$, which together with the term $k_{Pad}\eta_{Pad}$ have the same behaviour explained for the sleeper radiation; this was previously analysed through coefficients b_1, b_2 and b_3 of Eq. (16) in Fig. 9. Finally, increasing the rail foot width implies greater rail and total noise levels and the interaction effect $w_{\text{Foot}}k_{Pad}$ represents the same phenomenon that was explained for the rail radiation. In summary and for the sake of better understanding, the total sound power is represented as a function of the important design variables in Fig. 13.

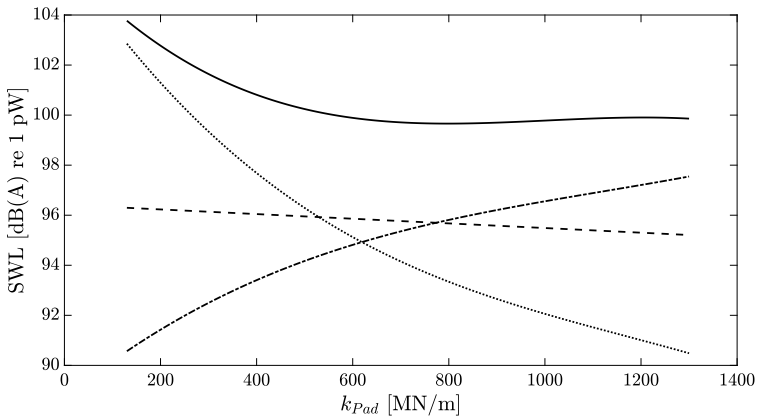

Fig. 12: Influence of rail pad stiffness on sound power level. ——: total; - - -: wheel component; ·····: rail component; -·-·-: sleeper component. The other contributing variables take medium values in their ranges.

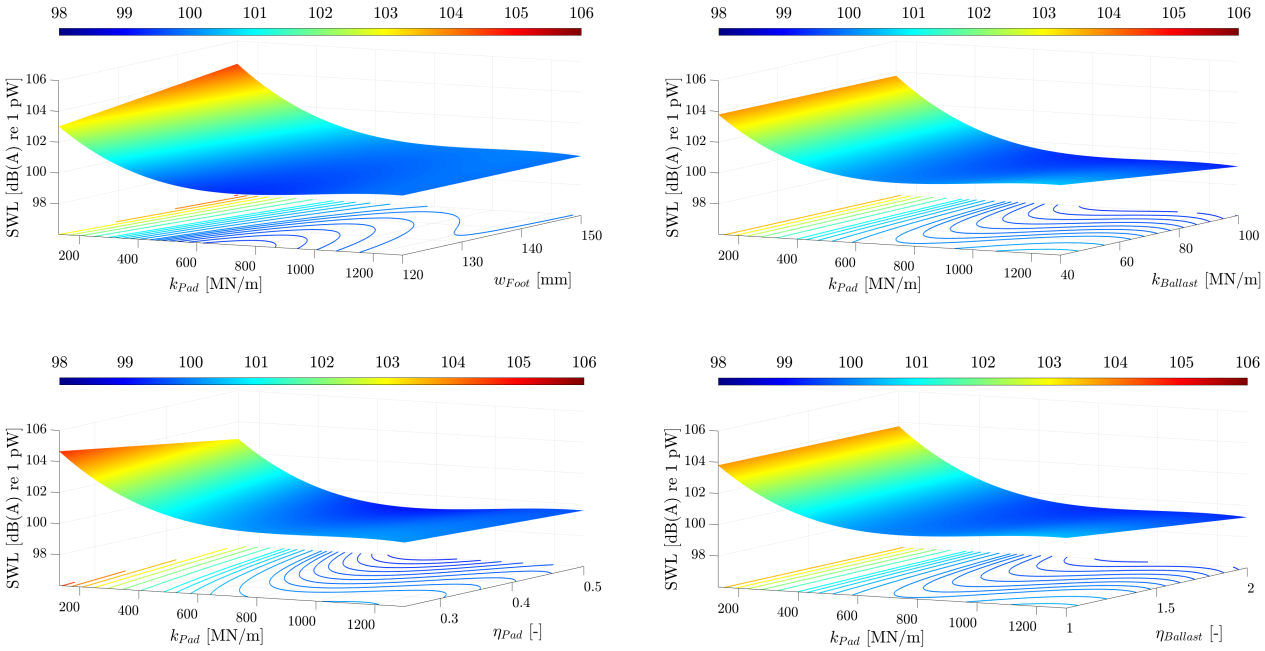

Fig. 13: Response surfaces of total sound power level for each important interaction of design variables. Parameters not represented take medium values in their ranges.

The regression model predicts that the optimal track design is reached with the following parameters: $w_{Foot} = 120$ mm, $k_{Pad} = 780$ MN/m, $\eta_{Pad} = 0.5$, $k_{Ballast} = 100$ MN/m and $\eta_{Ballast} = 2$, with a total sound power of 98.4 dB(A). In contrast, the worst design corresponds to the following parameters: $w_{Foot} = 150$ mm, $k_{Pad} = 130$ MN/m, $\eta_{Pad} = 0.25$, $k_{Ballast} = 40$ MN/m and $\eta_{Ballast} = 1$, with a sound power of 105.8 dB(A). Therefore, there is a difference between the best and the worst combination of 7.4 dB(A). Fig. 14 shows the TDR in vertical direction and the total sound power levels, both evaluated for the track design with the worst combination of parameters and with the optimal one. The TDR has been computed

in accordance with the standard EN15461 [31] using the track dynamic model of Section 2.2 and the acoustic radiation using the implemented tool of Section 2. Below about 2 kHz, in the frequency range in which the track contribution to the total noise is important, an inverse correlation between both variables can be appreciated. However, above about 2 kHz, the wheel contribution to the total noise makes it more difficult to correlate the TDR and total sound power radiation.

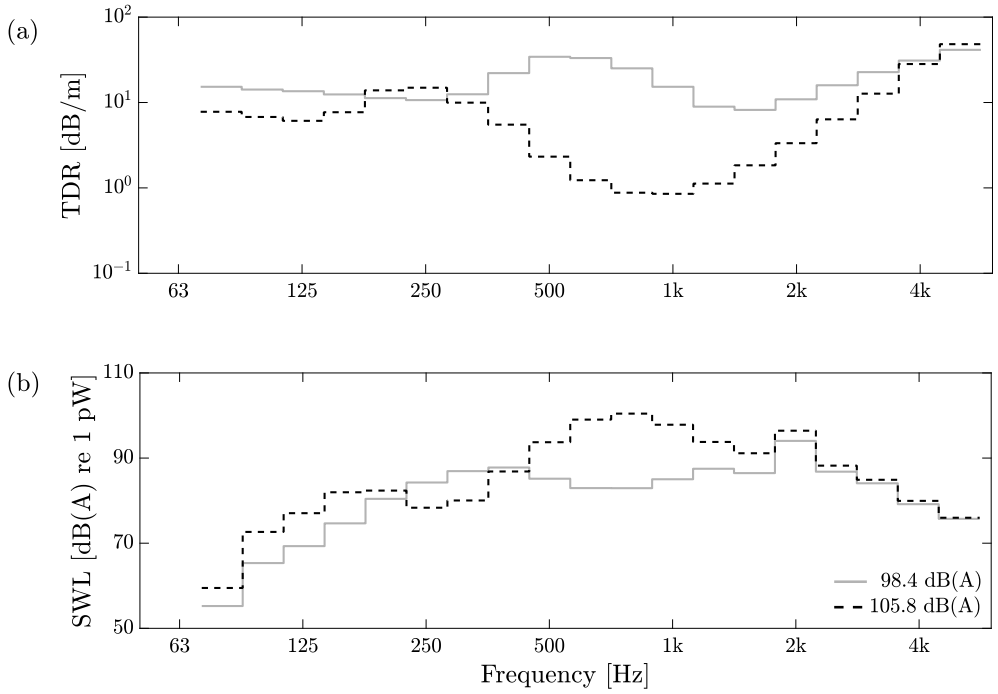

Fig. 14: Track Decay Rate in vertical direction (a) and total sound power level (b). ——: Optimal track design; - - -: Worst track design.

5. Conclusions

A vibroacoustic model of the railway wheel and track has been implemented which allows the sound power radiated by the wheel, rail and sleeper to be calculated as a consequence of the wheel/rail interaction. Then, the Pratt methodology has been used to analyse in detail the influence of the track design on the railway acoustic radiation.

To do this, a geometric parameterization of the rail cross-section has been carried out according to the European rails specified by the standard EN13674-1. Considering six geometric parameters of the rail as well as the stiffness and damping of the rail pad and ballast (in total ten variables), a design of experiments has been carried out that allows the influence of these variables on the sound radiation of the different railway components to be determined.

The analysis of the results shows that the railway sound radiation is governed mainly by the viscoelastic properties of the rail pad and ballast; the only influencing geometric parameter is the rail foot width. For the total radiation, a regression model has been developed which allows explaining 99.4 % of its variance. By far the most influential parameter is the

rail pad stiffness, followed by, in descending order, the rail pad damping, rail foot width, ballast stiffness and ballast damping.

The minimum sound power levels are found with: intermediate/high values of the rail pad stiffness, having a compromise between the rail, sleeper and wheel radiation (a similar conclusion was found in [20]); maximum values of the rail pad damping, reducing the rail and sleeper radiation; minimum values of the rail foot width, giving a lower radiation of the rail, and maximum values of the ballast stiffness and damping, reducing the sleeper radiation. Within the ranges of these five parameters, there is a difference between the best and the worst combination of 7.4 dB(A). However, this noise reduction is subject to the following considerations: (1) the calculations are for one speed and one roughness spectrum, (2) the range of rail pad stiffnesses in particular may not be acceptable to the track engineers for reasons other than noise pollution and (3) the narrower rail foot would require a modified rail fastening as it would be in greater danger of rail roll-over and would increase the mechanical stresses in that region of the rail putting its integrity at risk of fatigue.

6. Acknowledgements

This paper is part of the project PID2020-112886RA-I00 funded by MCIN/AEI/10.13 039/501100011033 and grant FPU18/03999 funded by MCIN/AEI/10.13039/501100011033 as well as by "ESF Investing in your future". The authors also acknowledge Programa PROMETEO/2021/046 of Generalitat Valenciana.

References

[1] T. Münzel, S. Kröller-Schön, M. Oelze, T. Gori, F. P. Schmidt, S. Steven, O. Hahad, M. Röösli, J. M. Wunderli, A. Daiber, M. Sørensen, Adverse cardiovascular effects of traffic noise with a focus on nighttime noise and the new WHO noise guidelines, Annual Review of Public Health 41 (1) (2020) 309–328, doi: http://doi.org/10.1146/annurev-publhealth-081519-062400.

[2] D. J. Thompson, Railway Noise and Vibration. Mechanisms, Modelling and Means of Control, Elsevier, 2009, ISBN: 978-0-08-045147-3.

[3] X. Zhang, D. J. Thompson, E. Quaranta, G. Squicciarini, An engineering model for the prediction of the sound radiation from a railway track, Journal of Sound and Vibration 461 (2019) 114921, doi: https://doi.org/10.1016/j.jsv.2019.114921.

[4] D. J. Thompson, N. Vincent, Track dynamic behaviour at high frequencies. Part 1: Theoretical models and laboratory measurements, Vehicle System Dynamics 24 (sup1) (1995) 86–99, doi: http://doi.org/10.1080/00423119508969617.

[5] P. J. Remington, Wheel/rail noise, part iv: Rolling noise, Journal of Sound and Vibration 46 (3) (1976) 419–436, doi: http://doi.org/10.1016/0022-460X(76)90864-6.

[6] D. J. Thompson, G. Squicciarini, J. Zhang, I. Lopez Arteaga, E. Zea, M. Dittrich, E. Jansen, K. Arcas, E. Cierco, F. X. Magrans, A. Malkoun, E. Iturritxa, A. Guiral, M. Stangl, G. Schleinzer, B. Martin Lopez, C. Chaufour, J. Wändell, Assessment of

measurement-based methods for separating wheel and track contributions to railway rolling noise, Applied Acoustics 140 (2018) 48–62, doi: http://doi.org/10.1016/j.apacoust.2018.05.012.

[7] J. C. O. Nielsen, Acoustic optimization of railway sleepers, Journal of Sound and Vibration 231 (3) (2000) 753–764, doi: http://doi.org/10.1006/jsvi.1999.2560.

[8] D. J. Thompson, P. E. Gautier, Review of research into wheel/rail rolling noise reduction, Proceedings of the Institution of Mechanical Engineers, Part F: Journal of Rail and Rapid Transit 220 (4) (2006) 385–408, doi: https://doi.org/10.1243/0954409JRRT79.

[9] J. C. O. Nielsen, C. R. Fredö, Multi-disciplinary optimization of railway wheels, Journal of Sound and Vibration 293 (2006) 510–521, doi: http://doi.org/10.1016/j.jsv.2005.08.063.

[10] X. Garcia-Andrés, J. Gutiérrez-Gil, J. Martínez-Casas, F. D. Denia, Wheel shape optimization approaches to reduce railway rolling noise, Structural and Multidisciplinary Optimization 62 (2020) 2555–2570, doi: https://doi.org/10.1007/s00158-020-02700-6.

[11] C. J. C. Jones, D. J. Thompson, Rolling noise generated by railway wheels with viscoelastic layers, Journal of Sound and Vibration 231 (3) (2000) 779–790, doi: https://doi.org/10.1006/jsvi.1999.2562.

[12] J. Färm, Evaluation of wheel dampers on an intercity train, Journal of Sound and Vibration 267 (3) (2003) 739–747, doi: https://doi.org/10.1016/S0022-460X(03)00737-5.

[13] C. Gramowski, T. Gerlach, Entering the real operation phase: design, construction and benefit verification of freight wheel noise absorber, Proceedings of 13th International Workshop on Railway Noise, Ghent, September 2019, pp. 16–20.

[14] F. Létourneaux, J. F. Cordier, F. Poisson, N. Douarche, High speed railway noise: assessment of mitigation measures, in: B. Schulte-Werning, *et al.* (Eds.), Proceedings of 9th International Workshop on Railway Noise, Munich, Germany, 4–8 September 2007, Notes on Numerical Fluid Mechanics & Multidisciplinary Design 99, 2008, pp. 56–62.

[15] D. J. Thompson, C. J. C. Jones, T. P. Waters, D. Farrington, A tuned damping device for reducing noise from railway track, Applied Acoustics 68 (1) (2007) 43–57, doi: http://doi.org/10.1016/j.apacoust.2006.05.001.

[16] B. Asmussen, D. Stiebel, P. Kitson, D. Farrington, D. Benton, Reducing the noise emission by increasing the damping of the rail: results of a field test, in: B. Schulte-Werning, *et al.* (Eds.), Proceedings of 9th International Workshop on Railway Noise, Munich, Germany, 4–8 September 2007, Notes on Numerical Fluid Mechanics & Multidisciplinary Design 99, 2008, pp. 229–235.

[17] W. Sun, D. J. Thompson, M. Toward, M. Wiseman, E. Ntotsios, S. Byrne, The influence of track design on the rolling noise from trams, Applied Acoustics 170 (2020) 107536, doi: http://doi.org/10.1016/j.apacoust.2020.107536.

[18] C. Gramowski, P. Suppin, Impact of rail dampers on the mainline rail roughness development, in: B. Schulte-Werning, *et al.* (Eds.), Proceedings of 12th International Workshop on Railway Noise, Terrigal, Australia, 12–16 September 2016, Notes on Numerical Fluid Mechanics & Multidisciplinary Design 139, 2018, pp. 367–374.

[19] C. J. C. Jones, D. J. Thompson, Means of controlling rolling noise at source, in: V. V. Krylov (Ed.), Noise and vibration from high-speed trains, Thomas Telford Ltd, London, 2001, Ch. 6, pp. 163–183, doi: http://doi.org/10.1680/navfht.29637.0006.

[20] N. Vincent, P. Bouvet, D. J. Thompson, P. E. Gautier, Theoretical optimization of track components to reduce rolling noise, Journal of Sound and Vibration 193 (1) (1996) 161–171, doi: http://doi.org/10.1006/jsvi.1996.0255.

[21] D. J. Thompson, B. Hemsworth, N. Vincent, Experimental validation of the TWINS prediction program for rolling noise, part 1: description of the model and method, Journal of Sound and Vibration 193 (1) (1996) 123–135, doi: http://doi.org/10.1006/jsvi.1996.0252.

[22] D. J. Thompson, P. Fodiman, H. Mahé, Experimental validation of the TWINS prediction program for rolling noise, part 2: results, Journal of Sound and Vibration 193 (1) (1996) 137–147, doi: http://doi.org/10.1006/jsvi.1996.0253.

[23] D. J. Thompson, Wheel-rail noise generation, part ii: Wheel vibration, Journal of Sound and Vibration 161 (3) (1993) 401–419, doi: http://doi.org/10.1006/jsvi.1993.1083.

[24] D. J. Thompson, Wheel-rail noise generation, part iii: Rail vibration, Journal of Sound and Vibration 161 (3) (1993) 421–446, doi: http://doi.org/10.1006/jsvi.1993.1084.

[25] Railway applications – Track – Rail – Part 1: Vignole railway rails 46 kg/m and above. EN 13674-1:2011+A1:2017, European Committee for Standardization (2017).

[26] D. C. Montgomery, Design and Analysis of Experiments, 10th Edition, John Wiley & Sons, Inc., 2019, ISBN: 978-1-119-49244-3.

[27] J. W. Pratt, Dividing the indivisible: Using simple symmetry to partition variance explained, Proceedings of the Second International Conference in Statistics, University of Tampere, Tampere, Finland, 1987, pp. 245–260.

[28] D. J. Thompson, C. J. C. Jones, Sound radiation from a vibrating railway wheel, Journal of Sound and Vibration 253 (2) (2002) 401–419, doi: http://doi.org/10.1006/jsvi.2001.4061.

[29] D. J. Thompson, M. H. A. Janssens, F. G. de Beer, Track Wheel Interaction Noise Software (TWINS) Theoretical Manual (version 3.4), TNO report, TNO Institute of Applied Physics, 2019.

[30] D. J. Mead, A general theory of harmonic wave propagation in linear periodic systems with multiple coupling, Journal of Sound and Vibration 27 (2) (1973) 235–260, doi: http://doi.org/10.1016/0022-460X(73)90064-3.

[31] Railway applications – Noise emission – Characterisation of the dynamic properties of track sections for pass by noise measurements. EN 15461:2008+A1:2010, European Committee for Standardization (2010).

[32] E. Salomons, Computational Atmospheric Acoustics, Kluwer, 2001, ISBN: 978-1-4020-0390-5.

[33] D. J. Thompson, C. J. C. Jones, N. Turner, Investigation into the validity of two-dimensional models for sound radiation from waves in rails, The Journal of the Acoustical Society of America 113 (2003) 1965–1974, doi: http://doi.org/10.1121/1.1555612.

[34] Railway applications – Wheelsets and bogies – Monobloc wheels – Technical approval procedure – Part 1: Forged and rolled wheels. EN 13979-1:2020, European Committee for Standardization (2020).

[35] D. J. Thompson, Wheel-rail noise generation, part i: Introduction and interaction model, Journal of Sound and Vibration 161 (3) (1993) 387–400, doi: http://doi.org/10.1006/jsvi.1993.1082.

[36] A. Johansson, J. C. O. Nielsen, R. Bolmsvik, A. Karlström, R. Lundén, Under sleeper pads—influence on dynamic train–track interaction, Wear 265 (2008) 1479–1487, doi: http://doi.org/10.1016/j.wear.2008.02.032.

[37] N. Vincent, D. J. Thompson, Track dynamic behaviour at high frequencies. part 2: Experimental results and comparisons with theory, Vehicle System Dynamics 24 (sup1) (1995) 100–114, doi: http://doi.org/10.1080/00423119508969618.

[38] Electroacoustics – Sound level meters – Part 1: Specifications. IEC 61672-1:2013, International Electrotechnical Commission (2013).

[39] D. R. Thomas, E. Hughes, B. D. Zumbo, On variable importance in linear regression, Social Indicators Research 45 (1/3) (1998) 253–275, doi: http://doi.org/10.1023/A:1006954016433.

[40] D. R. Thomas, P. C. Zhu, Y. J. Decady, Point estimates and confidence intervals for variable importance in multiple linear regression, Educational and Behavioral Statistics 32 (1) (2007) 61–91, doi: http://doi.org/10.3102/1076998606298037.

[41] D. J. Thompson, C. J. C. Jones, T. X. Wu, A. de France, The influence of the non-linear stiffness behaviour of rail pads on the track component of rolling noise, Proceedings of the Institution of Mechanical Engineers, Part F: Journal of Rail and Rapid Transit 213 (4) (1999) 233–241, doi: http://doi.org/10.1243/0954409991531173.